1   # Response of microbial community function to fluctuating

2   # geochemical conditions within a legacy radioactive waste trench

3   # environment

4   Xabier Vázquez-Campos[1,2], Andrew S. Kinsela[1,3], Mark W. Bligh[1,3], Jennifer J. Harrison[3],

5   Timothy E. Payne[3] & T. David Waite[1*]

6

7   [1]UNSW Water Research Centre and School of Civil and Environmental Engineering, The

8   University of New South Wales, Sydney, New South Wales 2052, Australia

9   [2]NSW Systems Biology Initiative, School of Biotechnology and Biomolecular Sciences, The

10   University of New South Wales, Sydney, New South Wales 2052, Australia

11   [3]Institute for Environmental Research, Australian Nuclear Science and Technology

12   Organisation, Locked Bag 2001, Kirrawee DC, New South Wales 2232, Australia

13

14   AEM

15   (Submitted March 2017)

16

17   Conflict of interest: The authors declare no conflict of interest.

18

19   *Corresponding author: Professor T.D. Waite; Email: d.waite@unsw.edu.au

Abstract

During the 1960s, small quantities of radioactive materials were co-disposed with chemical waste at the Little Forest Legacy Site (Sydney, Australia) in three-metre-deep, unlined trenches. Chemical and microbial analyses, including functional and taxonomic information derived from shotgun metagenomics, were collected across a six-week period immediately after a prolonged rainfall event to assess how changing water levels impact upon the microbial ecology and contaminant mobility. Collectively, results demonstrated that oxygen-laden rainwater rapidly altered the redox balance in the trench water, strongly impacting microbial functioning as well as the radiochemistry. Two contaminants of concern, plutonium and americium, were shown to transition from solid-iron-associated species immediately after the initial rainwater pulse, to progressively more soluble moieties as reducing conditions were enhanced. Functional metagenomics revealed the potentially important role that the taxonomically-diverse microbial community played in this transition. In particular, aerobes dominated in the first day followed by an increase of facultative anaerobes/denitrifiers at day four. Towards the mid-end of the sampling period, the functional and taxonomic profiles depicted an anaerobic community distinguished by a higher representation of dissimilatory sulfate reduction and methanogenesis pathways. Our results have important implications to similar near-surface environmental systems in which redox cycling occurs.

Importance

The role of chemical and microbiological factors in mediating the biogeochemistry of groundwaters from trenches used to dispose of radioactive materials during the 1960s is examined in this study. Specifically, chemical and microbial analyses, including functional and taxonomic information derived from shotgun metagenomics, were collected across a six-week period immediately after a prolonged rainfall event to assess how changing water levels influence microbial ecology and contaminant mobility.

Results demonstrate that oxygen-laden rainwater rapidly altered the redox balance in the trench water, strongly impacting microbial functioning as well as the radiochemistry. Two contaminants of concern, plutonium and americium, were shown to transition from solid-iron-associated species immediately after the initial rainwater pulse, to progressively more soluble moieties as reducing conditions were enhanced. Functional metagenomics revealed the important role that the taxonomically-diverse microbial community played in this transition. Our results have important implications to similar near-surface environmental systems in which redox cycling occurs.

Keywords: shotgun metagenomics, radionuclides, plutonium, americium, functional profile.

Introduction

57

58   The rapid expansion of an emerging nuclear industry immediately following World

59   War II resulted in substantial volumes of low-level radioactive waste (LLRW) being

60   generated from nuclear fuel cycle, weapons production, medical radioisotope and

61   radiochemical research activities. Although there was no consensus at this time, low-level

62   waste (and in some cases more active material) was commonly disposed of by burial in

63   shallow trenches, as evidenced in the United States at Maxey Flats (1), Oak Ridge (2) and

64   Hanford (3, 4); Canada at Chalk River (5); in the United Kingdom at Harwell (6) and LLRW

65   (7); in Lithuania at Maišiagala (8); and more recently in Ukraine at Chernobyl (9) to name

66   but a few. This was also the case for Australia's only nuclear (research) reactor at Lucas

67   Heights. Known as the Little Forest Legacy Site (LFLS), radioactive materials, including

68   minor amounts of $^{239+240}$Pu and ^{241}Am were placed in narrow (0.6 m), 3 m deep, unlined

69   trenches from 1960 to 1968 (10–12). Large volumes of contaminated non-radioactive

70   materials and equipment were also disposed of in these trenches (10).

71   The LFLS trenches were excavated within undisturbed geological matrices of red-

72   brown and grey clay (primarily kaolinite and illite/smectite) derived from the underlying

73   weathered shale, interspersed with minor phases of hematite and goethite (11, 13). The site

74   was chosen in part due to the low hydraulic conductivities of these materials (~ 9 to 66

75   mm/day) in order to isolate the LLRW from waters associated with the local hydrology cycle

76   (10–12). However, an unintended consequence of this (also experienced at other disposal

77   sites) has been that periodic intense rainfall and prolonged dry conditions can facilitate

78   complete saturation and desaturation of the more permeable waste material via surface

79   infiltration and evapo(transpi)ration/leakage mechanisms, respectively. Elaborating further,

80   this frequently results in infiltrating water filling up the more porous trenches to the surface

81   (akin to a 'bathtub'), which has been shown to be a primary mechanism for the dispersion of

4

82   contaminants $^{239+240}$Pu and ^{241}Am (10). Furthermore, this has allowed for redox cycling to

83   occur unabated in the LLRW trenches since their construction, potentially promoting redox

84   tolerant plasticity in the microbial communities present (14).

85   With actinide mobility, in many instances, strongly dependent on their oxidation state

86   (15), microbial communities can potentially play decisive roles in determining the fate and

87   mobility of such elements in the environment. In general, microbial communities can

88   influence actinide chemistry by partaking in redox (16–18), dissolution (19, 20), precipitation

89   (21, 22), sorption (23) and/or methylation (24) reactions, which may either enhance or retard

90   contaminant mobility.

91   Despite this, much of the scientific research to date has focussed on isolated individual

92   species (such as *Geobacter*, *Shewanella* and *Clostridium*) and their impact on actinide,

93   particularly uranium, behaviour. The challenge remains as to how best to identify the role of

94   microorganisms and their functioning within the wider microbial community which may be

95   undergoing external, environmental changes (25). Furthermore, subsurface environments

96   such as aquifers and shallow groundwaters, aside from being poorly studied, have been

97   shown to be havens for microbial novelty not dominated by the well-characterised organisms

98   listed above (26). Culture-independent techniques, such as metagenomics, in which genomic

99   sequences capture the aggregate microbial ecology of a sample (27, 28) have the potential to

100   enhance our understanding of these complex biogeochemical systems.

101   The question remains at LFLS, and in similar contaminated redox-cycling

102   environments, as to what function microbial communities may be performing in the direct or

103   indirect mobilisation and/or retention of legacy radionuclides. As the establishment of

104   causality between the legacy contaminants and microbial communities cannot be achieved in

105   such a non-invasive environmental study, the aim of this research was to understand the role

106   that periodic inundation from a large rainfall event, and presumably oxygen penetration, had

107 on the concomitant changes to chemistry-radiochemistry and microbial communities in a

108 LLRW trench environment. The two contaminants of major concern, Pu and Am, were the

109 focus of this research with shotgun metagenomics used to examine the microbial systems

110 function and taxonomy.

Materials and methods

111

Sample collection

112

113 Trench water samples were collected on five separate occasions across a two-month

114 period from LFLS. They were obtained from a screened PVC pipe which extends 1.55 m

115 below the ground surface. This pipe provides the only point of access into the legacy trenches

116 and was opportunistically installed during the partial collapse of the trench surface. Further

117 details of the trench sampler have been previously described in the literature (10, 29). Briefly,

118 a peristaltic pump operating under low flow rate was used to purge the borehole until

119 chemical parameters, particularly pH and oxidation/reduction potential (ORP), became stable

120 (Supplementary File 1). Measurements were made using a multi-probe system (YSI 556

121 MPS) coupled to a 100 mL flow cell. Stability usually took between 30 and 60 min, after

122 which sample collection began. Chemical parameters, along with the water depth, were

123 monitored over the sampling period (typically some hours) on the day of sampling to ensure

124 the water was representative of that particular period. The stability of flow cell parameters

125 and the fact that the water level did not decrease during the collection of 4–5 L of sample

126 material provides assurance that the samples were representative of the particular event rather

127 than anomalous local conditions.

128 The sample collection period commenced (on 23rd April 2015) immediately after a

129 substantial rainfall event, during which ~220 mm of rain fell over 3 days (Figure S1). Trench

130 water samples were subsequently collected on the 27th and 29th April, 14th May and 9th June

131   (or days 0, 4, 6, 21 and 47, post-rain, Figure S1).

132   Samples for chemical analyses were collected both with and without an in-line filtration

133   membrane (0.45 μm PES, Waterra FHT-Groundwater) in pre-washed and trench water rinsed

134   HDPE bottles except samples for organic carbon analysis which were collected in glass

135   bottles. Samples for radiochemical and cation analyses were acidified using double-distilled

136   HNO_3. All samples were then stored at 4 °C until analysis.

137   Samples for microbial analyses were collected by directly filtering the trench water

138   using a sterile PES 0.22 μm syringe filter (Sterivex-GP, Merck Millipore) with the volumes

139   of filtrate passing through the membranes recorded (410.1±82.2 mL per replicate, mean ±

140   SD). Filters were capped on site before being stored at -18 °C until analysis. Microbial

141   sampling was performed in triplicate to assess inherent variation.

142   Due to regulatory protocols governing sampling at the site, no solid phase material

143   could be extracted from the trenches. As the surrounding geological materials into which the

144   trenches were excavated provide little resemblance both physically and chemically to the

145   deposited waste within the trenches, they were discarded as providing useful information for

146   this study. As such all sampling within the trenches pertains to the extraction of soluble or

147   suspended solid-phases from the screened borehole.

148   **Chemical analyses of trench waters**

149   The primary radiochemical contaminants, $^{239+240}$Pu and ^{241}Am, were separated from

150   other radiochemical fractions using TEVA™ and TRU™ resin cartridges (30) before

151   measuring activity by alpha spectroscopy using a Canberra Alpha Analyst system coupled

152   with Passive Implanted Planar Silicon detectors (Canberra).

153   Cations (including Si, S and P) were measured by either ICP-AES or ICP-MS

154   depending on relative concentration. Anions (F^-, Cl^-, Br^-, I^-, PO_4^{3-} and NO_3^-) were determined

7

155   by ion chromatography (Dionex DX-600 IC System).

156   Non-purgeable dissolved organic carbon (0.45 µm filtered) was measured on freshly-

157   collected replicate samples by combustion catalytic oxidation (TOC-5000A, Shimadzu) with

158   concentration determined by a five-point calibration using newly-prepared potassium

159   hydrogen phthalate solutions.

160   Ferrous iron concentrations from 0.45 µm filtered samples were preserved in the field

161   with ammonium acetate-buffered phenanthroline solution (31). The absorbance of Fe(II) was

162   measured at 510 nm (USB4000, Ocean Optics) calibrated against a freshly-prepared

163   ammonium ferrous sulfate solution.

164   In field measurements of dissolved sulfide were attempted using methylene blue

165   colorimetry, but were consistently below detection limits (~1 µM) at all sampling time points.

166   All chemical analyses were performed in triplicate.

167   **DNA extraction and sequencing**

168   The PowerLyzer® PowerSoil® DNA Isolation kit (MO BIO) was used to extract DNA

169   from Sterivex filters following the modified protocol of Jacobs et al (32). Bead beating was

170   performed singularly in a PowerLyzer® 24 Bench Top Bead-Based Homogenizer (MO BIO)

171   at 2000 rpm for 5 min.

172   Concentration and DNA quality was evaluated with LabChip® GX (PerkinElmer).

173   Libraries were prepared with the TruSeq Nano DNA Library Preparation Kit and sequenced

174   in a NextSeq 500 (Illumina) with a 2×150 bp high output run. Output consisted of paired-end

175   reads with a median insert size of ~480 nt. Reads were deposited at the European Nucleotide

176   Archive (PRJEB14718/ERG009353).

177   **Data processing and functional analyses**

178   Raw   sequencing   reads   were   pre-processed   with   Trim   Galore!

8

179   (http://www.bioinformatics.babraham.ac.uk/projects/trim_galore/)   to   remove   residual

180   adapters as well as short and low quality sequences (Phred33 ≥ 20) while keeping unpaired

181   reads.

182   Taxonomic profiles were obtained from shotgun metagenomic data by extracting 16S

183   rDNA gene sequences with GraftM v0.10.1 (https://github.com/geronimp/graftM) and

184   mapping them with the 97% clustered GreenGenes database provided by GraftM developers

185   (package 4.39).

186   Functional analyses of the metagenomic data were performed with HUMAnN2 v0.6.0

187   (33). Gene families were grouped by MetaCyc reactions (RXN), keeping unmapped and

188   ungrouped reads for calculating copies per million and relative abundances. MetaCyc RXN

189   groups were filtered and only those with at least two replicates from the same sampling time-

190   point with a relative abundance of 10^{-4} or higher were analysed (33). MetaCyc RXN

191   notations have been used as is within Results and Discussion to provide an exact match with

192   the database. RXNs can be considered equivalent to the more traditionally used KO terms

193   from the KEGG database.Grouping by GO terms, specifically performed to evaluate virus

194   presence, indicated values under the threshold levels for all the virus-specific GO terms

195   identified. As such, viruses were not taken in further consideration.

196   Analysis of variance was performed with the software package STAMP v2.1.3 (34)

197   using the Benjamini-Hochberg False Discovery Rate approach (35) for correction of *p*-

198   values.

Results and Discussion

Water level changes and chemical analyses

201   The initial 220 mm rainfall event resulted in trenches filling to capacity and discharging

202   from the surface or porous near-surface (0–0.2 m) in the 'bathtub' mechanism described by

9

203   Payne et al (10) (Figure S1). Despite the subsequent 47-day sampling period receiving a

204   further 72 mm of rainfall, which periodically increased trench water levels, an overall decline

205   in trench water levels was observed across the sampling period (Figure S1).

206   Across the sampling period and as the water level declined, the pH was observed to

207   increase from 6.30 to 6.60, whereas the E_h values decreased from 247 to 147 mV (Figure 1).

208   Of the cations and anions analysed (Figure 2), iron displayed one of the greatest variations in

209   concentration, increasing from 0.42 mM at day 0, to 1.00 mM by day 47. The elevated

210   concentrations of iron are unsurprising, given that the LLRW at LFLS was disposed of in-

211   part within ~760 steel drums (36), and buried within a highly weathered shale geological

212   matrix (11). The continuous presence of Fe(II), even at day 0, confers reducing conditions in

213   excess of E_h values recorded, casting uncertainty over the absolute values supplied by the E_h

214   probe. The increase in Fe(II) concentrations with time was likely due to Fe(III) oxyhydroxide

215   reduction, an observation supported by the concurrent liberation of Si and P, two elements

216   that are typically co-associated with Fe(III)-oxyhydroxide at LFLS (37). The constant

217   concentrations of expected conservative elements Cl⁻ and K suggest that the drop in the

218   trench water level was due to subsurface outflow rather than evaporative processes across the

219   course of sampling. Other important elemental transitions included a 10-fold decrease in

220   dissolved sulfur concentrations (presumed to be sulfate), from an initial concentration of 62.4

221   to 6.2 µM at day 47 (Figure 2). Nitrate concentrations doubled between days 0 and 6 (from

222   0.24 to 0.55 µM) after which they decreased to below detection limits at days 21 and 47

223   (Figure 2).

224   The total (unfiltered) [241]Am activity increased from 15.7 to 27.8 Bq/L (1.8-fold

225   increase) while the soluble (filtered) fraction increased 3.4-times (7.2 to 24.7 Bq/L) between

226   days 0 and 47 (Figure 3). Although the activity of the total [239+240]Pu showed a proportionally

227   smaller increase than [241]Am across the sampling period, from 30.4 to 45.6 Bq/L (1.5 times),

10

228   the soluble fraction increased from 0.21 at day 0 and reached a maximum of 0.80 (35.1 Bq/L)

229   by day 21. Despite the low-flow sampling conditions, the majority of ^{241}Am and $^{239+240}$Pu in

230   the trench water was solid-associated at Day 0. This implies that the solid-associated

231   actinides are relatively stable or easily (re)mobilised, and also that during the rapid influx of

232   rainwater when the trenches are filling up (and potentially overspilling), colloidal transport is

233   likely to be the major form of contaminant movement at this site. Previous redox state

234   measurements at LFLS found that Pu was present in the Pu(IV) (64.5%) and colloidal/Pu(III)

235   (35.5%) states whilst Am was present exclusively as Am(III) (29). The vast quantities of

236   Fe(II) as well as the results of ancillary measurements (DO, ORP) would suggest that Pu(IV)

237   and Am(III) were again the dominant oxidation states of the trench water contaminants. The

238   results of all water quality parameters measured are provided in Table 1.

239   **Community composition**

240   Community profiles showed that *Bacteria* dominated over *Archaea* in the trench water

241   across the entire sampling period. A total of 70 phyla out of the 85 included in the

242   GreenGenes database were detected at some point and 11 phyla with values over 1% of the

243   total community at all times. Eukarya were found in low (~1% to ~2%), nearly constant

244   abundance trough the samples. Similarly, eukaryotic-specific RXNs were all below our

245   threshold significance level. As such they are not considered in further detail nor for the taxa

246   abundance numbers throughout the manuscript.

247   Archaea oscillated between 2.6 and 10.6% of the classified reads with minimum and

248   maximum at days 4 and 47, respectively. *Micrarchaeota* and *Parvarchaeota* (DPANN) were

249   the most abundant phyla at all times with a combined 45.5–55.9% of *Archaea*, while

250   remaining sequences were shared in variable proportions between the TACK superphylum

251   and *Euryarchaeota* (Figure 4). Although the fraction of TACK decreased over time from

252   24.8% at day 0 to 12.4% at day 47, *Euryarchaeota* reached a maximum at day 47

253 contributing 37.2% of all *Archaea*. These changes were derived mainly from variations in the

254 SAGMA-X family (*Thaumarchaeota*), related to the ammonia oxidising archaeon 'Ca.

255 Nitrosotalea' (38, 39) and, in *Bathyarchaeota* (MCG), which includes the only potential non-

256 euryarchaeal methanogens (39, 40) and/or one of the few acetogenic *Archaea* (41). The

257 increase in total *Archaea* abundance over time was related to changes to and ANME-2d,

258 *Methanoregulaceae* and *Methanosaetaceae* families, implicated in methane metabolism (42–

259 44) as well as the *Micrarchaeota* and *Parvarchaeota* phyla.

260 Only 8 bacterial phyla grouped more than 5% of the total bacterial reads at any one

261 sampling point, and amongst them, only *Chloroflexi*, OD1 (*Parcubacteria*), OP11

262 (*Microgenomates*), OP3 (*Omnitrophica*) and *Proteobacteria* were within the 10 most

263 abundant bacterial phyla at all times (Figure 4). The principal changes observed over time

264 refer to *Proteobacteria*, TM7 (*Saccharibacteria*), OP3, *Acidobacteria* and OD1. While the

265 proportion of TM7 and *Acidobacteria* decreased from day 0, both OP3, and OD1 reached

266 their maximum by day 47 (18.9% and 14.7%). The *Proteobacteria*, often the most abundant

267 phylum, showed a conspicuous increase, mainly due to *Betaproteobacteria*, comprising

268 48.7% of all classified reads at day 4. The order *Burkholderiales* was identified as being

269 primarily responsible for this change (42.6% of total), esp. the genus *Ralstonia* (20.3%)

270 within *Oxalobacteraceae* (34.0%). These bacteria were also responsible for the altered

271 functional profile observed at day 4.

272 Several studies focusing on the microbiology of groundwater or subsurface ecosystems

273 have demonstrated the existence of organisms able to pass through standard 0.22 µm filters

274 (45–47). Despite this, a substantial portion of the Little Forest trench water community

275 corresponded to taxa known to be able to pass through 0.22 µm filters, i.e. OD1, OP11 and

276 DPANN. We suggest this could be derived from the fast precipitation of iron in our extracted

277 trench waters, effectively entrapping cells, or that they were attached to colloidal particles or

278   to other cells. Still, it is possible that the numbers for these 'ultra-small' taxa could be

279   underestimated in our results.

280   A complete taxonomic profile of all sample replicates at each individual time point is

281   provided in Supplementary Information. An important aside to be noted with this data is the

282   inherent reproducibility between sample triplicates. This finding provides a level of

283   reassurance with regards to the aggregate nature of these water samples, often neglected in

284   similar studies.

Carbon cycling

286   Initial time points were characterised by a significantly ($p \leq 0.05$) higher relative

287   abundance of RXNs using molecular dioxygen as substrate such as: cytochrome-c oxidase

288   (CYTOCHROME-C-OXIDASE-RXN,   EC:1.9.3.1,   Figure   5A),   quinol–cytochrome-c

289   reductase (1.10.2.2-RXN) and several mono- and dioxygenases. This was combined with a

290   significantly ($p \leq 0.05$) lower relative abundance of methanogenesis-related RXNs,

291   nitrogenase (ferredoxin, NITROGENASE-RXN), rubisco (RIBULOSE-BISPHOSPHATE-

292   CARBOXYLASE-RXN),   or   heterolactic   fermentation   (PHOSPHOKETOLASE-RXN).

293   Catalase (CATAL-RXN, EC:1.11.1.6/21, see Reactive oxygen species detoxification in SI)

294   gene relative abundance was highest at day 4 along with several ABC transporters and

295   phosphotransferases, e.g. D-ribopyranose, D-xylose, spermidine or L-arginine, as well as

296   assimilatory sulfur and nitrogen pathway RXNs (refer to SI for details). The higher relative

297   abundances of all these genes at day 4 suggest a metabolism more dependent on oxygen, i.e.

298   aerobic, or at least microaerophilic (see Nitrogen cycling). It also confers a higher

299   dependence on available organic carbon (viz. heterotrophy), or on the presence of decaying

300   complex organic matter (48). These interpretations are collectively supported by the

301   geochemical measurements including the higher E_h values, decreasing concentrations of

302   sulfur and absence of nitrate, along with lower iron concentrations across the first sampling

13

303   points.

304   Regarding the source of the organic fraction, the results suggest that soil particles and

305   associated organo-chemicals were mobilised from material above the trenches via advective

306   transport mechanisms during and immediately after rainfall. This was evidenced by the

307   increased proportion of soil-associated *Actinobacteria* at day 0, which diminished to 0.71%

308   by day 4 (Figure 4). Furthermore, the presence of genes encoding for enzymes representing

309   chitin degradation, such as chitobiase (RXN-12625, EC:3.2.1.52), diminished progressively

310   until day 47 indicating a potential one-off provision of chitin, matching the leaching

311   hypothesis (Figure S2). In addition, numerous facultative and strict anaerobes can degrade

312   chitin and/or chitobiose (49–51), which lessens the likelihood of the alternative hypothesis

313   that chitin depletion could be derived from the intrinsic lack of chitobiase in anaerobes.

314   The other primary biopolymer found in soil is cellulose (52). The relative abundance of

315   cellulase (RXN-2043, EC:3.2.1.4) showed no significant differences between days 0, 21 and

316   47 ($p = 0.172$) suggesting a consistent supply of cellulose (Figure 5B). The exception, noted

317   at day 4, can be explained by the proliferation of *Burkholderiales*. The constant abundance of

318   cellulose is unsurprising given the historical records which indicate a range of organic

319   (particularly cellulose-based) compounds were co-disposed of in the LFLS trenches (11).

320   This hypothesis accords with previous stable isotope measurements, which identified the

321   degradation of legacy organic matter as being responsible for enriched $\delta^{13}C$ (inorganic)

322   values measured near the trench (11).

323   Lignin is present to a lesser or greater extent in all plant biomass. From the list of

324   enzymes in the literature capable of degrading lignin (53, 54), only below-threshold levels of

325   certain genes were detected: versatile peroxidase (RXN0-267, EC:1.11.1.16), dye peroxidase

326   (RXN-11813, EC:1.11.1.19) and laccase (LACCASE-RXN, EC:1.10.3.2). The overall lack of

327   genes for proteins capable of lignin degradation strengthens the hypothesis that trench waste

14

328   material is the source of cellulosic material rather than being derived from the degradation of

329   plant material from the topsoil.

330   The two fundamental genes representing the glyoxylate pathway, isocitrate lyase

331   (ISOCIT-CLEAV-RXN, EC:4.1.3.1, Figure S3) and malate synthase (MALSYN-RXN,

332   EC:4.1.3.2, Figure 5C) showed between 3–4 times higher relative abundance in days 0 and 4

333   when compared to day 47. This pathway facilitates the use of short chain carbon compounds

334   (C2–C3) for anabolic purposes, compounds especially generated during anaerobic processes.

335   Although the glyoxylate pathway genes have been previously detected in organisms living in

336   anaerobic environments (55), it was absent from strict anaerobic organisms based on the

337   results from EggNOG (56), KEGG (57) and UniProtKB (58) databases (as of 24/05/2017).

338   This finding supports the hypothesis that trench waters became anoxic as the water level

339   declined, promoting conditions which favour the development of strict anaerobes.

340   Furthermore, the aerobic community which developed immediately after the rainfall event

341   likely utilised (and benefited from) the short chain carbon compounds generated by preceding

342   anaerobic conditions.

343   Both acetoclastic and hydrogenotrophic methanogenesis pathways were evident from

344   the functional profile analysis. Similar maximum relative abundances, about $1.4 \cdot 10^{-4}$, of 5-

345   methyltetrahydrosarcinapterin:corrinoid/iron-sulfur protein *Co*-methyltransferase (RXN-

346   12908, EC:2.1.1.245, Figure 5D) and coenzyme F_{420}-dependent hydrogenase (COENZYME-

347   F420-HYDROGENASE-RXN, EC:1.12.98.1, Figure S4), which are specific RXNs for the

348   methanogenesis from acetate and H_2 and CO_2, were observed at day 47. The presence of

349   methanogenesis-specific RXNs is supported by previous isotopic measurements, showing

350   δ^2H enrichment, relative to $\delta^{18}O$, in the vicinity of the trenches (11). Concurrently, the

351   taxonomy revealed the presence of the ANME-2d division contributing up to 13.8% of all

352   *Archaea* at day 47 (1.5% of the community). The ANME-2d division was initially linked to

353   the anaerobic oxidation of methane using NO_3^- (42) or even NO_2^- (59), constituting one of the

354   primary methane sinks in anaerobic conditions. However, recent research has shown that

355   some of the members of this taxa are able to utilise Fe(III) in place of NO_2^- or NO_3^- (44, 60,

356   61). This provides a more reasonable explanation given the limited nitrate present and

357   abundance of iron during the later sampling days.

358   **Sulfur cycling**

359   The relative abundance of sulfite cytochrome *c* reductase (SULFITE-

360   DEHYDROGENASE-RXN, EC:1.8.2.1, Figure S5), involved in the assimilatory reduction of

361   sulfate, peaked at day 4, with ~10 times higher relative abundance compared to day 0. At the

362   same time, dissimilatory sulfate reduction RXNs, e.g. dissimilatory sulfite reductase

363   (HYDROGENSULFITE-REDUCTASE-RXN, EC:1.8.99.3), followed the opposite trend,

364   with a maximum at day 47 (Figure 5E). The combined relative abundance of all the putative

365   sulfate reducing bacteria (SRB) taxa detected (mainly *Syntrophobacterales*,

366   *Thermodesulfovibrionaceae* and *Desulfobacterales*) also increased over time, from 2.3% of

367   the total prokaryotes at day 0 to 4.9% at day 47. Dissimilatory sulfate reduction is one of the

368   major redox processes in both natural (62) and artificial (63) anaerobic environments. The

369   ten-fold reduction in the sulfur concentration is thought to result from the loss of dissolved

370   sulfate via reduction to sulfide and subsequent precipitation of insoluble heavy metal sulfides,

371   particularly FeS. This interpretation is supported by the lack of measurable sulfides in the

372   trench water (see Chemical analyses of trench waters), along with previous reports showing

373   sulfate reduction based on isotopic fractionation and severe (10 to 100-fold) depletion in

374   sulfate concentrations in trench waters relative to surrounding wells (11). The potential

375   contribution of sulfate- and nitrite-dependent anaerobic methane oxidation (S-DAMO and N-

376   DAMO respectively) was discounted due to the near complete absence of ANME taxa

377   (*Archaea*) aside from ANME-2d, and NC10 (*Bacteria*) (see Nitrogen cycling) (44, 59, 64,

16

378   65).

379   **Nitrogen cycling**

380   The (inorganic) nitrogen cycle was mostly represented by RXNs related to

381   denitrification and assimilatory nitrogen reactions, primarily dissimilatory nitrate reductase

382   (RXN-16471, EC:1.7.5.1, see Figure S6 for a complete profile of the N-associated RXNs),

383   although nitrogen fixation (NITROGENASE-RXN, EC:1.18.6.1) was the predominant N-

384   associated RXN. All other prominent N-associated RXNs peaked at day 4 with the exception

385   of hydroxylamine reductase (HYDROXYLAMINE-REDUCTASE-RXN, EC:1.7.99.1) and

386   ammonia oxygenase (AMONITRO-RXN, EC:1.14.99.39). The increase in nitrate

387   concentrations observed between days 4 and 6 (0.236 and 0.552 µM respectively) might be

388   derived from the oxidation of NO by nitric oxide dioxygenase (R621-RXN, EC:1.14.12.17).

389   This surge in the relative abundance of nitrogen metabolism RXNs (at day 4) coincided with

390   an increased dominance of *Betaproteobacteria*, mostly *Burkholderiales*. *Betaproteobacteria*

391   have been linked to denitrification processes in a uranium-polluted aquifer in Rifle (USA)

392   (66) and they may play a similar ecological role at LFLS. However, the increase in nitrate

393   concentrations could equally be indicative of NO or NO_2^- oxidation, originally produced by

394   the aerobic oxidation of ammonium by the *Thaumarchaeota* (67, 68).

395   The inorganic nitrogen cycling results provide important information regarding the

396   transition from aerobic to anaerobic conditions as the water level declines. The competing

397   requirements of nitrate respiration, which necessitates oxygen-limiting conditions at a

398   minimum (69), and NO dioxygenase needing molecular oxygen, collectively suggest that at

399   day 4 the trench waters were no longer aerobic, but more likely microaerophilic/hypoxic.

400   However, many facultative anaerobes are capable of using nitrate as an alternate electron

401   acceptor when oxygen is not available. As such, the high relative abundance of nitrate

402   reducing enzyme genes at day 4 (viz. dissimilatory nitrate reductases) could be a confounding

403   effect associated with the increased abundance of *Burkholderiales*. This was confirmed by

404   searching the denitrifying pathway in KEGG (map00910) (as of 08/07/2016) (57).

405   **Iron cycling**

406   Temporal increases in Fe(II) concentrations, such those experienced in the later anoxic

407   periods of the sampling, may be associated with the use of Fe(III) during anaerobic

408   respiration, previously attributed to decaheme *c*-type cytochromes from the OmcA/MtrC

409   family present in iron-reducing bacteria (FeRB) such as *Shewanella* spp. and *Geobacter* spp.

410   (70). However, their representation in the trench water metagenome data was scarce (relative

411   abundance $\leq 10^{-6}$). It is known that for respiration to occur, FeRB often require direct

412   physical contact with Fe(III) solids (71). As only aqueous/suspended phase sampling was

413   permissible at LFLS, it is possible the under representation of a FeRB community was due to

414   our sampling regime in which the solid-phase was largely excluded.

415   The genes associated with RXNs specific to the Fe(II) oxidation pathway (via

416   rusticyanin, PWY-6692): ubiquinone-cytochrome-*bc1* reductase (EC:1.10.2.2, RXN-15829)

417   and *aa3*-type cytochrome oxidase (EC:1.9.3.1, RXN-15830) were present, despite no iron-

418   rusticyanin reductase (EC:1.16.9.1, RXN-12075), *cyc2*, being found under the established

419   threshold (maximum value $\sim 3 \times 10^{-6}$) (72). The presence of both cytochromes could be

420   because HUMAnN2 could not distinguish between the 'generic' quinol–cytochrome-c

421   reductase (RXN-15816, EC:1.10.2.2), and cytochrome *c* oxidase (CYTOCHROME-C-

422   OXIDASE-RXN) respectively, particularly when analysing short reads.

423   The presence of 1.9% of *Gallionellaceae* (over the total community composition) at

424   day 0 and 2.9% of *Crenothrix*, a non-FeOB usually associated with Fe-mineralising biofilms

425   (73), suggest the existence of transient microaerophilic iron oxidising activity in the trench

426   water despite the extremely low relative abundance of *cyc2*. Waste disposal records from

18

427 LFLS indicate that numerous steel drums (~760) were co-disposed of in the trenches (36).

428 Based on the active sulfate respiration observed in the trench waters, we would expect that

429 iron/steel materials may have suffered microbially induced corrosion (MIC) (74), potentially

430 contributing to the elevated Fe(II) concentrations. However, the main iron MIC product is

431 likely FeS (74), which can be utilised by *Gallionella ferruginea* (*Gallionellaceae*), an iron

432 oxidising bacterium (FeOB) (75). Furthermore, this process would also provide an

433 explanation for a persistent source of Fe(III) (oxy)hydroxides and their ongoing interaction

434 with the S-cycle.

435 Previous research on soils experiencing fluctuating redox conditions and active iron

436 cycling have shown they frequently lack 'typical' Fe(III)-respiring bacteria (76), being

437 outcompeted by sulfate respiration (77). Despite Fe(III) being a more thermodynamically

438 favourable electron acceptor it is commonly acknowledged that sulfate respiration often

439 outcompetes Fe(III) respiration in both high and low sulfate environments (77, 78). High

440 levels of sulfate reduction in low-sulfate environments, akin to the LFLS trenches, has been

441 previously observed to occur in the presence of crystalline Fe(III) oxyhydroxides that

442 partially re-oxidise sulfide generated by SRB to elemental sulfur (78). This mechanism

443 provides a plausible explanation for our observations at LFLS. The large concentration of

444 dissolved Fe(II) in the trench waters would likely contribute to the Fe(II)-catalysed

445 transformation of amorphous ferrihydrite to more crystalline, thermodynamically-favourable

446 forms (79, 80), although this would be limited to some extent by the large concentrations of

447 dissolved organic matter and silica (81). Furthermore, the abiotic reduction of crystalline

448 Fe(III) oxyhydroxides would severely limit the energy acquisition by FeRB and therefore the

449 FeRB would only outcompete SRB when sulfate and other reducible sulfur compounds were

450 totally consumed.

451 Alternatively, fermentative bacteria coupling the oxidation of a range of organic

452   compounds to the reduction of ferric iron (82–84) may play an integral role in maintaining

453   the elevated Fe(II) concentrations observed within the trenches. One example is the organism

454   *Propionibacterium freudenreichii* which has previously been observed to reduce Fe(III) by

455   using humic substances as an electron mediator (85). In this regard, both heterolactic and

456   propionic acid fermentation pathways showed high relative abundances based on

457   phosphoketolase (PHOSPHOKETOLASE-RXN, EC:4.1.2.9) and methylmalonyl-CoA

458   decarboxylase (RXN0-310, EC:4.1.1.41), respectively (Figure S7). Their decrease in relative

459   abundance (at day 4) could be explained by the lack of fermentative pathways present in the

460   genomes associated with the population shift, i.e. increase in *Burkholderiales*. This was

461   confirmed by searching (as of 08/06/2016) methylmalonyl-CoA decarboxylase and

462   phosphoketolase in the KEGG maps (map00640 and map00030, respectively).

463   **Synthesis of trench processes and radiochemical mobilisation implications**

464   The biogeochemistry of this dynamic system is conceptually described by the elemental

465   cycling schematic shown in Figure 6. Immediately following the rainfall event, the E_h

466   reached its most oxidising value (247 mV) with the microbial community characterised by

467   higher relative abundances of pathways related to aerobic (or at least microaerophilic)

468   heterotrophic metabolism and one capable of chitin degradation. Although conditions were

469   not strongly oxidising, this pulse of oxic water would be sufficient to induce the abiotic

470   oxidation of part of the large store of dissolved Fe(II), likely forming a combination of the

471   reactive Fe(III) oxyhydroxides ferrihydrite and silica-ferrihydrite, along with the more

472   crystalline oxyhydroxide lepidocrocite, as has previously been observed in these trench

473   waters (37). As both Am(III) and Pu(III)/(IV) are known to strongly sorb to sediments and

474   iron oxides (15), it is of little surprise to observe the greatest proportions of (suspended)

475   solid-associated actinides at this time point (day 0, Figure 3). Note that even though most Am

476   (54.3%) and particularly Pu (78.8%) were associated with a solid-fraction >0.45 µm, they

477   were still extracted from the trench under our low-flow sampling method. This finding

478   implies that colloid-associated Pu, and to a lesser extent Am, remains mobile within the

479   trench waters, congruent with observations from other legacy radioactive waste sites (86).

480   Interestingly though, the Pu migration distance away from source at LFLS in groundwater

481   has been shown to be much smaller (~1 order of magnitude less) compared to other legacy

482   locations such as the Nevada Test Site (87), Rocky Flats (88) and Mayak (89). We attribute

483   this to a low permeability soil matrix, inhibiting downward migration to the

484   connected/permanent water table, coupled with the biogeochemical conditions within the

485   trenches themselves. The high concentrations of Fe(II), circumneutral pH and proliferation of

486   aerobic heterotrophs drives the rapid formation of large quantities of Fe(III) oxides. The

487   quantity of Fe(III) oxides that form upon oxic rainwater intrusion is evidently sufficient to

488   contain the bulk of contaminants within the trenches during 'bathtub' overflow events. The

489   rate of Fe(II) oxidation is likely to be crucial for the ongoing attenuation of Pu and Am at

490   LFLS (37).

491   By day 4, as water levels rapidly decrease, an increase of *Burkholderiales*

492   (*Betaproteobacteria*) generates a functional profile disturbance and, while the aerobic profile

493   is maintained, it is also the time-point at which nitrogen cycling (e.g. nitrate respiration)

494   becomes most active (Figure 6; ▯). Therefore, day 4 represents a potential transition away

495   from oxic conditions derived from rain infiltration, though this sequence of events is

496   somewhat confounded by the microbial growth lag phase associated with aerobic respirators.

497   Over the following weeks (days 21 and 47), the microbial community transitions to a

498   functional profile dominated by carbon fixation, methanogenesis and sulfate respiration

499   pathways (Figure 6; ▯▯▯▯). The increase in anaerobicity correlated with increasing

500   concentrations of soluble Fe and soluble radionuclides and a depletion of sulfate and nitrate.

501   In the case of Am, although the total activity increased gradually as the water level in the

502   trench declined, the soluble fraction increased by a greater proportion (Figure 3). This

503   indicates that either a desorption or dissolution process occurred. The concomitant increase in

504   the soluble Am fraction and Fe(II) concentrations point towards reductive dissolution of

505   Fe(III) oxyhydroxides as a major driver behind Am solubilisation.

506   The Pu behaviour in the trenches presents a more complex temporal dynamic due, in

507   part, to its more varied redox chemistry. As conditions become more reducing over time, one

508   would expect to observe soluble Pu activities increase, through both the dissolution of Fe(III)

509   oxides and, to a lesser extent, from Pu(IV) to Pu(III) reduction. In an interesting point of

510   difference to Am, our results show that Pu proportionally remained in the particle-associated

511   fraction for a substantially longer period, even as the dissolved Am(III) activity and Fe(II)

512   concentration increased. The reason for the differing solution/solid-phase partitioning

513   observed for Pu and Am is not clear based on the evidence to hand. The inability to sample

514   solid materials from within the trenches has limited more conclusive understanding.

515   However, we suggest the differing Am and Pu associations are likely due to different redox

516   states, based on the previous measurements at LFLS, which showed a dominant Pu oxidation

517   state of +4 (29). Electrostatically, Pu(IV), as the neutral hydrolysed cation $Pu(OH)_4(aq)$ or as

518   an intrinsic colloid, is more likely sorbed or incorporated into positively charged pseudo-

519   colloids such as Fe(III) oxides, compared to Am^{3+}. This is supported by research showing the

520   highly reversible nature of Am(III) sorption onto poor crystalline iron colloids (90) and

521   association with carbonate- and exchangeable sites on clays (91).

Conclusions

523   The inability to comprehensively access and sample within legacy radioactive waste

524   environments hampers our ability to comprehend co-occurring elemental cycling and

525   microbial metabolism, potentially curtailing our ability to effectively manage and remediate

526   such sites. The trench-sampling point at LFLS is therefore a particularly useful resource for

527   such research. In this study, our coupled use of metagenomics and chemical analyses has

528   provided a previously unattainable level of understanding for the LFLS trench water,

529   highlighting the responsiveness of the microbial community to external changes and dynamic

530   nature of the resulting chemistry. The combined results show that the trench waters contain a

531   taxonomically diverse microbial community, which has likely evolved in response to

532   variations in energy sources supplied by frequent redox fluctuations. When combined with

533   the complex nature of the waste-form, a myriad of micro-environments has developed within

534   the trenches, allowing for simultaneous O, N, Fe, S and C elemental cycling, as shown by co-

535   occurring metabolic reactions in the aggregate water samples. Consequently, it can be

536   inferred that Pu and Am are subject to persistent reducing conditions (as evident from active

537   iron oxide dissolution, sulfate reduction and methanogenesis) when the water level is low

538   between rainfall events. These reductive processes maintain Pu and Am solubility, despite the

539   occasional onset of oxidising conditions associated with rainfall events. Ultimately however,

540   the high concentrations of Fe present and the tendency of Fe(II) to be relatively rapidly

541   oxidised to strongly sorbing Fe(III) (oxy)hydroxide solids on exposure to oxic conditions

542   results in limited transport of Pu and Am.

543   Although the findings described above are intrinsically linked to the specific site under

544   investigation, they provide important generic insights into the dynamic biogeochemical

545   behaviour of iron-rich, redox-cycling environments. Of particular interest is the rapid

546   response of the microbial community to dynamic redox conditions and the potential impact

547   upon persistent contaminant solubility and enhanced mobility.

Acknowledgements

549   ANSTO staff members are thanked for their valuable contributions: Kerry Wilsher

550   (fieldwork, laboratory analyses), Sangeeth Thiruvoth (actinides), Brett Rowling (fieldwork,

551   inorganics), Henri Wong (inorganics), Chris Vardanega (inorganics) and Dioni Cendón

552   (discussion). The Australian Bureau of Meteorology is acknowledged for rainfall data.

553   ## Author contribution

554   Study concept and experimental design: XVC, ASK, TDW. Fieldwork: ASK. Chemical

555   and radiochemical analyses: ASK, JJH. Molecular biology and bioinformatics analyses:

556   XVC. Contribution of reagents/materials/analysis tools: TEP, TDW. Manuscript writing:

557   XVC, ASK. Revision and review of the manuscript: XVC, ASK, MWB, TDW.

558   ## References

559   1.   Cleveland JM, Rees TF. 1981. Characterization of plutonium in Maxey Flats radioactive trench leachates.
560   Science 212:1506–1509.

561   2.   Saunders JA, Toran LE. 1995. Modeling of radionuclide and heavy metal sorption around low- and high-
562   pH waste disposal sites at Oak Ridge, Tennessee. Appl Geochem 10:673–684.

563   3.   Cantrell KJ, Felmy AR. 2012. Plutonium and americium geochemistry at Hanford: a site-wide review.
564   RPT-DVZ-AFRI-001 PNNL-21651. Pacific Northwest National Laboratory, Washington (USA).

565   4.   Gerber MS. 1992. Past practices technical characterization study — 300 area — Hanford site. WHC-MR-
566   0388. UC-702. Westinghouse Hanford Company, Richland, WA.

567   5.   Killey RWD, Rao RR, Eyvindson S. 1998. Radiocarbon speciation and distribution in an aquifer plume
568   and groundwater discharge area, Chalk River, Ontario. Appl Geochem 13:3–16.

569   6.   Fellingham L, Graham A, Stiff S. 2003. Characterisation and remediation of beryllium waste pits in the
570   Southern storage area at Harwell, p. 1041–1049. *In* ASME 2003 9th International Conference on
571   Radioactive Waste Management and Environmental Remediation. American Society of Mechanical
572   Engineers, Oxford, England.

573   7.   Wilkins MJ, Livens FR, Vaughan DJ, Lloyd JR, Beadle I, Small JS. 2010. Fe(III) reduction in the
574   subsurface at a low-level radioactive waste disposal site. Geomicrobiol J 27:231–239.

575   8.   Gudelis A, Gvozdaitė R, Kubarevičienė V, Druteikienė R, Lukoševičius Š, Šutas A. 2010. On radiocarbon
576   and plutonium leakage to groundwater in the vicinity of a shallow-land radioactive waste repository. J
577   Environ Radioact 101:443–445.

578   9.   Bugai D, Kashparov V, Dewiére L, Khomutinin Y, Levchuk S, Yoschenko V. 2005. Characterization of
579   subsurface geometry and radioactivity distribution in the trench containing Chernobyl clean-up wastes.
580   Environ Geol 47:869–881.

581   10.   Payne TE, Harrison JJ, Hughes CE, Johansen MP, Thiruvoth S, Wilsher KL, Cendón DI, Hankin SI,
582   Rowling B, Zawadzki A. 2013. Trench 'bathtubbing' and surface plutonium contamination at a legacy
583   radioactive waste site. Environ Sci Technol 47:13284–13293.

584   11.   Cendón DI, Hughes CE, Harrison JJ, Hankin SI, Johansen MP, Payne TE, Wong H, Rowling B, Vine M,
585   Wilsher K, Guinea A, Thiruvoth S. 2015. Identification of sources and processes in a low-level
586   radioactive waste site adjacent to landfills: groundwater hydrogeochemistry and isotopes. Aust J Earth Sci
587   62:123–141.

588   12.   Hughes CE, Cendón DI, Harrison JJ, Hankin SI, Johansen MP, Payne TE, Vine M, Collins RN, Hoffmann
589   EL, Loosz T. 2011. Movement of a tritium plume in shallow groundwater at a legacy low-level
590   radioactive waste disposal site in eastern Australia. J Environ Radioact 102:943–952.

591   13.   Isaacs SR, Mears KF. 1977. A study of the burial ground used for radioactive waste at the Little Forest
592   area near Lucas Heights New South Wales. AAEC/E--427. Australian Atomic Energy Commission
593   Research Establishment, Lucas Heights, N.S.W. (AU).

594   14.   Pett-Ridge J, Firestone MK. 2005. Redox fluctuation structures microbial communities in a wet tropical
595   soil. Appl Environ Microbiol 71:6998–7007.

596   15.   Choppin GR. 2007. Actinide speciation in the environment. J Radioanal Nucl Chem 273:695–703.

597   16.   Kimber RL, Boothman C, Purdie P, Livens FR, Lloyd JR. 2012. Biogeochemical behaviour of plutonium
598   during anoxic biostimulation of contaminated sediments. Mineral Mag 76:567–578.

599   17.   Lloyd JR, Sole VA, Praagh CVGV, Lovley DR. 2000. Direct and Fe(II)-mediated reduction of technetium
600   by Fe(III)-reducing bacteria. Appl Environ Microbiol 66:3743–3749.

601   18.   Renshaw JC, Butchins LJC, Livens FR, May I, Charnock JM, Lloyd JR. 2005. Bioreduction of uranium:
602   Environmental implications of a pentavalent intermediate. Environ Sci Technol 39:5657–5660.

603   19.   Francis AJ, Dodge CJ, Gillow JB. 2008. Reductive dissolution of Pu(IV) by *Clostridium* sp. under
604   anaerobic conditions. Environ Sci Technol 42:2355–2360.

605   20.   Renshaw JC, Law N, Geissler A, Livens FR, Lloyd JR. 2009. Impact of the Fe(III)-reducing bacteria
606   *Geobacter sulfurreducens* and *Shewanella oneidensis* on the speciation of plutonium. Biogeochemistry
607   94:191–196.

608   21.   Fomina M, Charnock JM, Hillier S, Alvarez R, Gadd GM. 2007. Fungal transformations of uranium
609   oxides. Environ Microbiol 9:1696–1710.

610   22.   Wilkins MJ, Livens FR, Vaughan DJ, Beadle I, Lloyd JR. 2007. The influence of microbial redox cycling
611   on radionuclide mobility in the subsurface at a low-level radioactive waste storage site. Geobiology
612   5:293–301.

613   23.   Vázquez-Campos X, Kinsela AS, Collins RN, Neilan BA, Aoyagi N, Waite TD. 2015. Uranium binding
614   mechanisms of the acid-tolerant fungus *Coniochaeta fodinicola*. Environ Sci Technol 49:8487–8496.

615   24.   Amachi S, Fujii T, Shinoyama H, Muramatsu Y. 2005. Microbial influences on the mobility and
616   transformation of radioactive iodine in the environment. J Nucl Radiochem Sci 6:21–24.

617   25.   Bertin PN, Heinrich-Salmeron A, Pelletier E, Goulhen-Chollet F, Arsène-Ploetze F, Gallien S, Lauga B,
618   Casiot C, Calteau A, Vallenet D, Bonnefoy V, Bruneel O, Chane-Woon-Ming B, Cleiss-Arnold J, Duran
619   R, Elbaz-Poulichet F, Fonknechten N, Giloteaux L, Halter D, Koechler S, Marchal M, Mornico D,
620   Schaeffer C, Smith AAT, Van Dorsselaer A, Weissenbach J, Médigue C, Le Paslier D. 2011. Metabolic
621   diversity among main microorganisms inside an arsenic-rich ecosystem revealed by meta- and proteo-
622   genomics. ISME J 5:1735–1747.

623   26.   Castelle CJ, Hug LA, Wrighton KC, Thomas BC, Williams KH, Wu D, Tringe SG, Singer SW, Eisen JA,
624   Banfield JF. 2013. Extraordinary phylogenetic diversity and metabolic versatility in aquifer sediment. Nat
625   Commun 4:2120.

626   27.   Aguiar-Pulido V, Huang W, Suarez-Ulloa V, Cickovski T, Mathee K, Narasimhan G. 2016.
627   Metagenomics, metatranscriptomics, and metabolomics approaches for microbiome analysis. Evol
628   Bioinform 12:5–16.

629   28.   Allen EE, Banfield JF. 2005. Community genomics in microbial ecology and evolution. Nat Rev Micro
630   3:489–498.

631   29.   Ikeda-Ohno A, Harrison JJ, Thiruvoth S, Wilsher K, Wong HKY, Johansen MP, Waite TD, Payne TE.
632   2014. Solution speciation of plutonium and americium at an Australian legacy radioactive waste disposal
633   site. Environ Sci Technol 48:10045–10053.

634   30.   Harrison JJ, Zawadzki A, Chisari R, Wong HKY. 2011. Separation and measurement of thorium,
635   plutonium, americium, uranium and strontium in environmental matrices. J Environ Radioact 102:896–
636   900.

637   31.   APHA, AWWA, WEF. 1998. Standard methods for the examination of water and wastewater20th ed.
638   APHA-AWWA-WEF, Washington, D.C.

639   32.   Jacobs J, Rhodes M, Sturgis B, Wood B. 2009. Influence of environmental gradients on the abundance
640   and distribution of *Mycobacterium* spp. in a coastal lagoon estuary. Appl Environ Microbiol 75:7378–
641   7384.

642   33.   Abubucker S, Segata N, Goll J, Schubert AM, Izard J, Cantarel BL, Rodriguez-Mueller B, Zucker J,
643   Thiagarajan M, Henrissat B, White O, Kelley ST, Methé B, Schloss PD, Gevers D, Mitreva M,
644   Huttenhower C. 2012. Metabolic reconstruction for metagenomic data and its application to the human
645   microbiome. PLoS Comput Biol 8:e1002358.

646   34.   Parks DH, Tyson GW, Hugenholtz P, Beiko RG. 2014. STAMP: statistical analysis of taxonomic and
647   functional profiles. Bioinformatics 30:3123–3124.

648   35.   Benjamini Y, Hochberg Y. 1995. Controlling the False Discovery Rate: A Practical and Powerful
649   Approach to Multiple Testing. J Roy Stat Soc B 57:289–300.

650   36.   Payne TE. 2012. Background report on the Little Forest Burial Ground legacy waste site. ANSTO / E-
651   780. Institute for Environmental Research, Australian Nuclear Science and Technology Organisation,
652   Lucas Heights, N.S.W. (AU).

653   37.   Kinsela AS, Jones AJ, Bligh MW, Pham AN, Collins RN, Harrison JJ, Wilsher KL, Payne TE, Waite TD.
654   2016. Influence of dissolved silicate on Fe(II) oxidation. Environ Sci Technol 50:11663–11671.

655   38.   Jiang L, Zheng Y, Chen J, Xiao X, Wang F. 2011. Stratification of archaeal communities in shallow
656   sediments of the Pearl River Estuary, Southern China. Antonie van Leeuwenhoek 99:739–751.

657   39.   Meng J, Xu J, Qin D, He Y, Xiao X, Wang F. 2014. Genetic and functional properties of uncultivated
658   MCG archaea assessed by metagenome and gene expression analyses. ISME J 8:650–659.

659   40.   Evans PN, Parks DH, Chadwick GL, Robbins SJ, Orphan VJ, Golding SD, Tyson GW. 2015. Methane
660   metabolism in the archaeal phylum Bathyarchaeota revealed by genome-centric metagenomics. Science
661   350:434–438.

662   41.   He Y, Li M, Perumal V, Feng X, Fang J, Xie J, Sievert SM, Wang F. 2016. Genomic and enzymatic
663   evidence for acetogenesis among multiple lineages of the archaeal phylum Bathyarchaeota widespread in
664   marine sediments. Nat Microbiol 16035.

665   42.   Haroon MF, Hu S, Shi Y, Imelfort M, Keller J, Hugenholtz P, Yuan Z, Tyson GW. 2013. Anaerobic
666   oxidation of methane coupled to nitrate reduction in a novel archaeal lineage. Nature 500:567–570.

667   43.   Karakashev D, Batstone DJ, Trably E, Angelidaki I. 2006. Acetate oxidation is the dominant
668   methanogenic pathway from acetate in the absence of methanosaetaceae. Appl Environ Microbiol
669   72:5138–5141.

670   44.   Leu A, Hu S, Cai C, Yuan Z, Orphan VJ, Tyson GW. 2016. Understanding the metabolic potential of
671   ANME-2d and its role in anaerobic methane oxidation coupled to metal reduction. Montreal, Canada.

672   45.   Luef B, Frischkorn KR, Wrighton KC, Holman H-YN, Birarda G, Thomas BC, Singh A, Williams KH,
673   Siegerist CE, Tringe SG, Downing KH, Comolli LR, Banfield JF. 2015. Diverse uncultivated ultra-small
674   bacterial cells in groundwater. Nat Commun 6:6372.

675   46.   Baker BJ, Tyson GW, Webb RI, Flanagan J, Hugenholtz P, Allen EE, Banfield JF. 2006. Lineages of
676   acidophilic Archaea revealed by community genomic analysis. Science 314:1933–1935.

677   47.   Brown CT, Hug LA, Thomas BC, Sharon I, Castelle CJ, Singh A, Wilkins MJ, Wrighton KC, Williams
678   KH, Banfield JF. 2015. Unusual biology across a group comprising more than 15% of domain Bacteria.
679   Nature 523:208–211.

680   48.   Peng R-H, Xiong A-S, Xue Y, Fu X-Y, Gao F, Zhao W, Tian Y-S, Yao Q-H. 2008. Microbial
681   biodegradation of polyaromatic hydrocarbons. FEMS Microbiol Rev 32:927–955.

682   49.   Riemann L, Azam F. 2002. Widespread *N*-acetyl-D-glucosamine uptake among pelagic marine bacteria
683   and its ecological implications. Appl Environ Microbiol 68:5554–5562.

684   50.   Sorokin DY, Rakitin AL, Gumerov VM, Beletsky AV, Damsté S, S J, Mardanov AV, Ravin NV. 2016.
685   Phenotypic and genomic properties of *Chitinispirillum alkaliphilum* gen. nov., sp. nov., a haloalkaliphilic
686   anaerobic chitinolytic bacterium representing a novel class in the phylum *Fibrobacteres*. Front Microbiol
687   7.

688   51.   Zavarzina DG, Tourova TP, Kolganova TV, Boulygina ES, Zhilina TN. 2009. Description of
689   *Anaerobacillus alkalilacustre* gen. nov., sp. nov.—Strictly anaerobic diazotrophic bacillus isolated from
690   soda lake and transfer of *Bacillus arseniciselenatis*, *Bacillus macyae*, and *Bacillus alkalidiazotrophicus* to
691   *Anaerobacillus* as the new combinations *A. arseniciselenatis* comb. nov., *A. macyae* comb. nov., and *A.
692   alkalidiazotrophicus* comb. nov. Microbiology 78:723–731.

693   52.   Beier S, Bertilsson S. 2013. Bacterial chitin degradation—mechanisms and ecophysiological strategies.
694   Front Microbiol 4:149.

695   53.   de Gonzalo G, Colpa DI, Habib MHM, Fraaije MW. 2016. Bacterial enzymes involved in lignin
696   degradation. J Biotechnol 236:110–119.

697   54.   Pollegioni L, Tonin F, Rosini E. 2015. Lignin-degrading enzymes. FEBS J 282:1190–1213.

698   55.   Burow LC, Mabbett AN, Blackall LL. 2008. Anaerobic glyoxylate cycle activity during simultaneous
699   utilization of glycogen and acetate in uncultured *Accumulibacter* enriched in enhanced biological
700   phosphorus removal communities. ISME J 2:1040–1051.

701   56.   Huerta-Cepas J, Szklarczyk D, Forslund K, Cook H, Heller D, Walter MC, Rattei T, Mende DR,
702   Sunagawa S, Kuhn M, Jensen LJ, von Mering C, Bork P. 2016. eggNOG 4.5: a hierarchical orthology
703   framework with improved functional annotations for eukaryotic, prokaryotic and viral sequences. Nucl
704   Acids Res 44:D286–D293.

705   57.   Kanehisa M, Sato Y, Kawashima M, Furumichi M, Tanabe M. 2016. KEGG as a reference resource for
706   gene and protein annotation. Nucl Acids Res 44:D457–D462.

707   58.   Magrane M, Uniprot Consortium. 2011. UniProt Knowledgebase: a hub of integrated protein data.
708   Database 2011:bar009.

709   59.   Cui M, Ma A, Qi H, Zhuang X, Zhuang G. 2015. Anaerobic oxidation of methane: an "active" microbial
710   process. MicrobiologyOpen 4:1–11.

711   60.   Timmers PHA, Welte CU, Koehorst JJ, Plugge CM, Jetten MSM, Stams AJM. 2017. Reverse
712   methanogenesis and respiration in methanotrophic Archaea. Archaea 2017:e1654237.

713   61.   Ettwig KF, Zhu B, Speth D, Keltjens JT, Jetten MSM, Kartal B. 2016. Archaea catalyze iron-dependent
714   anaerobic oxidation of methane. PNAS 113:12792–12796.

715   62.   Grein F, Ramos AR, Venceslau SS, Pereira IAC. 2013. Unifying concepts in anaerobic respiration:
716   Insights from dissimilatory sulfur metabolism. Biochim Biophys Acta Bioenerg 1827:145–160.

717   63.   Paulo LM, Stams AJM, Sousa DZ. 2015. Methanogens, sulphate and heavy metals: a complex system.
718   Rev Environ Sci Biotechnol 14:537–553.

719   64.   Scheller S, Yu H, Chadwick GL, McGlynn SE, Orphan VJ. 2016. Artificial electron acceptors decouple
720   archaeal methane oxidation from sulfate reduction. Science 351:703–707.

721   65.   He Z, Cai C, Wang J, Xu X, Zheng P, Jetten MSM, Hu B. 2016. A novel denitrifying methanotroph of the
722   NC10 phylum and its microcolony. Sci Rep 6:32241.

723   66.   Wrighton KC, Castelle CJ, Wilkins MJ, Hug LA, Sharon I, Thomas BC, Handley KM, Mullin SW,
724   Nicora CD, Singh A, Lipton MS, Long PE, Williams KH, Banfield JF. 2014. Metabolic interdependencies
725   between phylogenetically novel fermenters and respiratory organisms in an unconfined aquifer. ISME J
726   8:1452–1463.

727   67.   Könneke M, Schubert DM, Brown PC, Hügler M, Standfest S, Schwander T, Borzyskowski LS von, Erb
728   TJ, Stahl DA, Berg IA. 2014. Ammonia-oxidizing archaea use the most energy-efficient aerobic pathway
729   for CO_2 fixation. PNAS 111:8239–8244.

730   68.   Pester M, Schleper C, Wagner M. 2011. The Thaumarchaeota: an emerging view of their phylogeny and
731   ecophysiology. Curr Opin Microbiol 14:300–306.

732   69.   Fischer M, Falke D, Pawlik T, Sawers RG. 2014. Oxygen-dependent control of respiratory nitrate
733   reduction in mycelium of *Streptomyces coelicolor* A3(2). J Bacteriol 196:4152–4162.

734   70.   Lovley DR, Holmes DE, Nevin KP. 2004. Dissimilatory Fe(III) and Mn(IV) reduction. Adv Microb
735   Physiol 49:219–286.

736   71.   Weber KA, Achenbach LA, Coates JD. 2006. Microorganisms pumping iron: anaerobic microbial iron
737   oxidation and reduction. Nat Rev Micro 4:752–764.

738   72.   Kato S, Ohkuma M, Powell DH, Krepski ST, Oshima K, Hattori M, Shapiro N, Woyke T, Chan CS. 2015.
739   Comparative genomic insights into ecophysiology of neutrophilic, microaerophilic iron oxidizing
740   bacteria. Front Microbiol 6.

741   73.   Emerson D, Fleming EJ, McBeth JM. 2010. Iron-oxidizing bacteria: an environmental and genomic
742   perspective. Ann Rev Microbiol 64:561–583.

743   74.   Anandkumar B, George RP, Maruthamuthu S, Parvathavarthini N, Mudali UK. 2016. Corrosion
744   characteristics of sulfate-reducing bacteria (SRB) and the role of molecular biology in SRB studies: an
745   overview. Corrosion Rev 34:41–63.

746   75.   Lütters-Czekalla S. 1990. Lithoautotrophic growth of the iron bacterium *Gallionella ferruginea* with
747   thiosulfate or sulfide as energy source. Arch Microbiol 154:417–421.

748   76.   DeAngelis KM, Silver WL, Thompson AW, Firestone MK. 2010. Microbial communities acclimate to
749   recurring changes in soil redox potential status. Environ Microbiol 12:3137–3149.

750   77.   Cozzarelli IM, Weiss JV. 2007. Biogeochemistry of Aquifer Systems, p. 843–859. *In* Hurst, CJ,
751   Crawford, RL, Garland, JL, Lipson, DA, Mills, AL, Stetzenbach, LD (eds.), Manual of environmental
752   microbiology. American Society of Microbiology.

753   78.   Hansel CM, Lentini CJ, Tang Y, Johnston DT, Wankel SD, Jardine PM. 2015. Dominance of sulfur-
754   fueled iron oxide reduction in low-sulfate freshwater sediments. ISME J 9:2400–2412.

755   79.   Boland DD, Collins RN, Miller CJ, Glover CJ, Waite TD. 2014. Effect of solution and solid-phase
756   conditions on the Fe(II)-accelerated transformation of ferrihydrite to lepidocrocite and goethite. Environ
757   Sci Technol 48:5477–5485.

758   80.   Pedersen HD, Postma D, Jakobsen R, Larsen O. 2005. Fast transformation of iron oxyhydroxides by the
759   catalytic action of aqueous Fe(II). Geochim Cosmochim Acta 69:3967–3977.

760   81.   Jones AM, Collins RN, Rose J, Waite TD. 2009. The effect of silica and natural organic matter on the
761   Fe(II)-catalysed transformation and reactivity of Fe(III) minerals. Geochim Cosmochim Acta 73:4409–
762   4422.

763   82.   Lovley D. 2013. Dissimilatory Fe(III)- and Mn(IV)-Reducing Prokaryotes, p. 287–308. *In* Rosenberg, E,
764   DeLong, EF, Lory, S, Stackebrandt, E, Thompson, F (eds.), The Prokaryotes. Springer Berlin Heidelberg,
765   Berlin, Heidelberg.

766   83.   Lovley DR, Phillips EJP. 1988. Novel mode of microbial energy metabolism: Organic carbon oxidation
767   coupled to dissimilatory reduction of iron or manganese. Appl Environ Microbiol 54:1472–1480.

768   84.   Straub KL, Benz M, Schink B. 2001. Iron metabolism in anoxic environments at near neutral pH. FEMS
769   Microbiol Ecol 34:181–186.

770   85.   Benz M, Schink B, Brune A. 1998. Humic acid reduction by *Propionibacterium freudenreichii* and other
771   fermenting bacteria. Appl Environ Microbiol 64:4507–4512.

772   86.   Kersting AB. 2013. Plutonium transport in the environment. Inorg Chem 52:3533–3546.

773   87.   Kersting AB, Efurd DW, Finnegan DL, Rokop DJ, Smith DK, Thompson JL. 1999. Migration of
774   plutonium in ground water at the Nevada Test Site. Nature 397:56–59.

775   88.   Santschi PH, Roberts KA, Guo L. 2002. Organic nature of colloidal actinides transported in surface water
776   environments. Environ Sci Technol 36:3711–3719.

777   89.   Novikov AP, Kalmykov SN, Utsunomiya S, Ewing RC, Horreard F, Merkulov A, Clark SB, Tkachev VV,
778   Myasoedov BF. 2006. Colloid transport of plutonium in the far-field of the Mayak Production
779   Association, Russia. Science 314:638–641.

780   90.   Schäfer T, Artinger R, Dardenne K, Bauer A, Schuessler W, Kim JI. 2003. Colloid-borne americium
781   migration in Gorleben groundwater: Significance of iron secondary phase transformation. Environ Sci
782   Technol 37:1528–1534.

783   91.   Lujanienė G, Beneš P, Štamberg K, Ščiglo T. 2012. Kinetics of plutonium and americium sorption to
784   natural clay. J Environ Radioact 108:41–49.

785

786 **Figure captions**

787 **Figure 1. pH and E_h (Standard Hydrogen Electrode corrected) measurements from the trench**

788 **water across the sampling period.**

789 **Figure 2. Temporal changes to element/ion concentrations in the trench water.** Bars show the

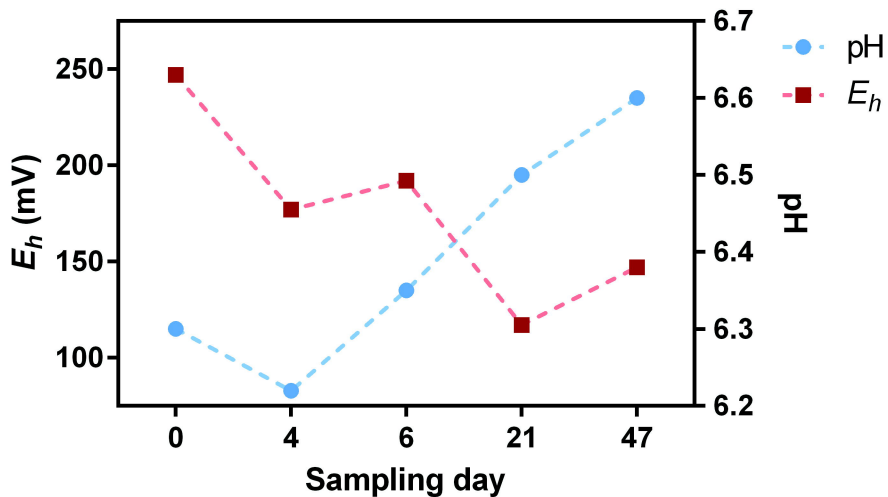790 individual concentrations of each element/ion over the five sampling days 0, 4, 6, 21 and 47.

791 **Figure 3. Activity of filtered and unfiltered radionuclides measured in the trench water.** Filtered

792 fractions (<0.45 µm, solid fill) are equivalent to soluble and smaller colloidal particles. Unfiltered

793 fractions (full bar) are as considered total (soluble plus all suspended solids) concentrations. Error

794 bars show the standard deviation of triplicate measurements.

795 **Figure 4. Taxa relative abundances over time.** Only taxa with an average relative abundance >5%

796 of the total sequences in at least a single sampling day are shown. Taxa with <5% of all sequences

797 are grouped under 'other'. Phyla with <5% of relative abundance at all times are grouped under 'other

798 phyla', except Archaea.

799 **Figure 5. Changes in the relative abundances of selected RXNs over time.** A, Cytochrome C

800 oxidase; B, cellulase; C, malate synthase; D, 5-methyltetrahydrosarcinapterin:corrinoid/iron-sulfur

801 protein Co-methyltransferase (CH3-HSPT:Fe-S protein Co-MT); E: sulfite reductase; and F,

802 superoxide dismutase.

803 **Figure 6. Hypothetical global scheme of the processes at LFLS.** Orange details on barrels

804 reading Fe(III) represent solid Fe(III) minerals, mainly (oxy)hydroxides. Colour of arrows represent the

805 time at which each process takes place: red, aerobic/after rain; brown, microaerophilic; blue,

806 anaerobic/dry phase; and black arrows indicate processes that seem to be independent from the

807 sampling time. Dashed arrows indicate transport. Abbreviations used in the figure: C_{org}, organic

808 carbon;   MIC,   microbially   induced   corrosion; CH_3-HSPT:Fe-S   protein   *Co*-MT,   5-

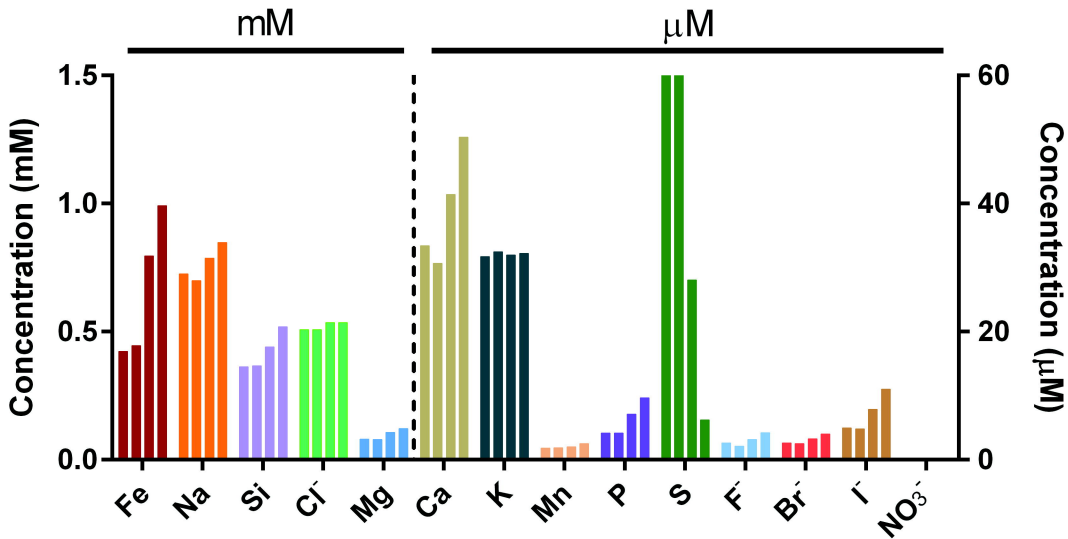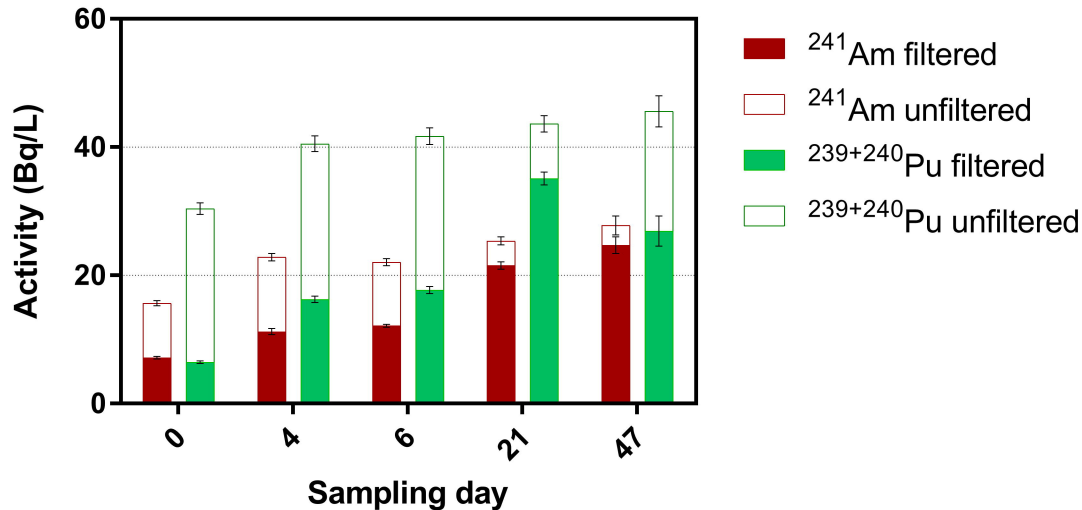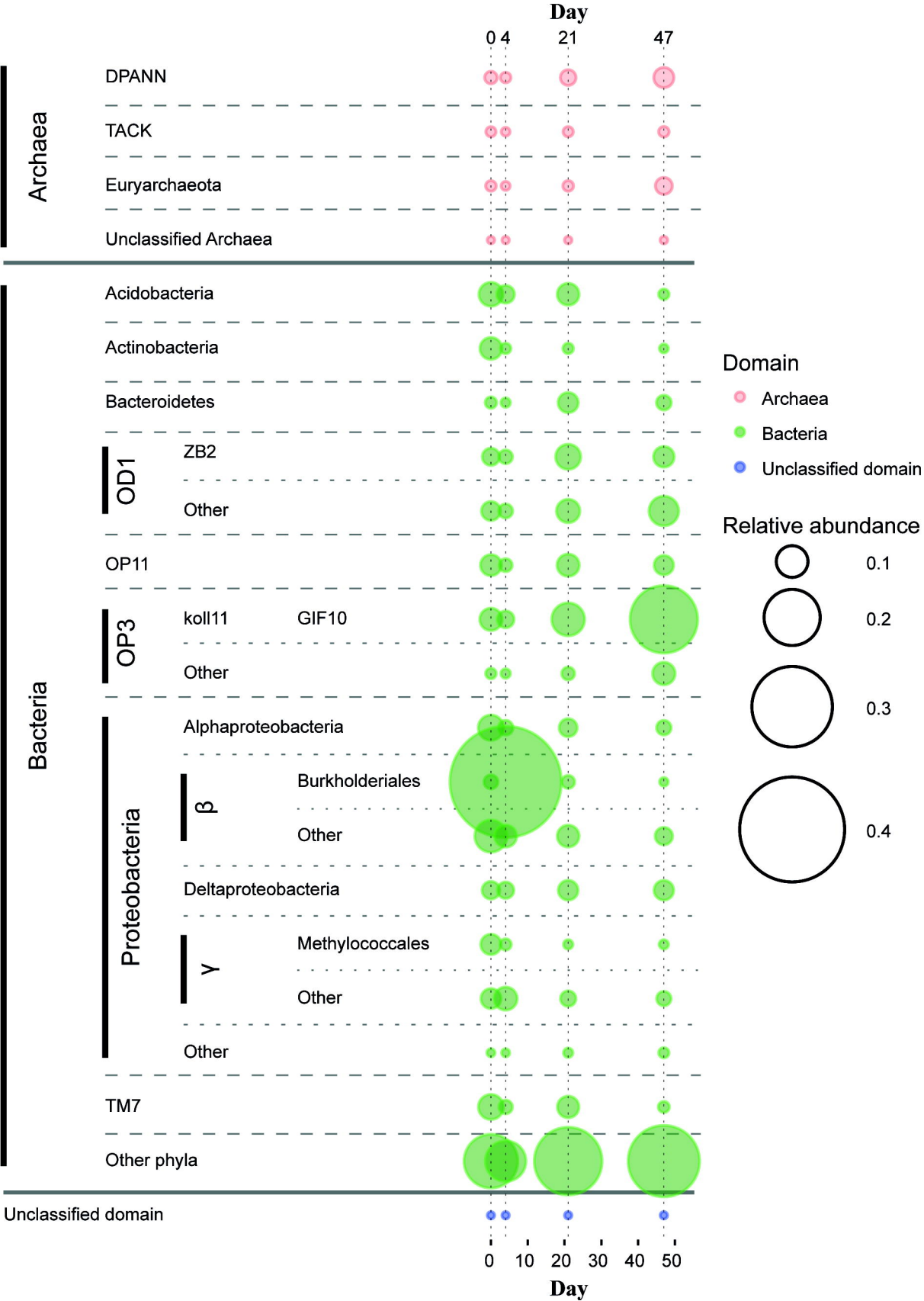809 methyltetrahydrosarcinapterin:corrinoid/iron-sulfur protein Co-methyltransferase.

Figure 3

Figure 5